Pseudo Sliding Mode Control with Integrative Action Applied to Brushless DC Motor Speed Control

José Roberto B. A. Monteiro, Carlos M. R. Oliveira, Thales E. P. Almeida, Marcel J. Cezare
School of Engineering of São Carlos - EESC
University of São Paulo
São Carlos, SP 13566-590
Email: jrm@sc.usp.br

***Abstract*—Although sliding mode control has many drawbacks when applied to electrical drives due to real limitations of switches, as limited frequency of operation, turn on and turn off delays, some of its theory can be succesfully used in order to project a high performance controller, robust and with a reduced design effort. This paper shows the use of sigmoidal function, hyperbolic tangent, instead of the signal function. So, it actually consists not in a pure but in a pseudo (or quasi) sliding mode, combined to an integrative controller action and with an anti-windup effect, so the result is a high performance controller, robust to machine parameters and disturbances, and light in its design. Results shows its high performance and robustness. The chosen sliding surface has integrative control action combined to an anti-windup feature, which zeroes the steady state error and minimizes the output system overshoot.**

Keywords*—*Quasi sliding Mode Control, brushless DC motor control, motor speed control.

I. Introduction

An ideal sliding mode does not exists in practice since it would imply that switches work at an infinite frequency. Due to real realizations of the switches, as a limited switching frequency and commutation delays, as well as limitations in the feedback control, such as discontinuities, discretization, and time delays, a particular dynamic behavior appears in the vicinity of the sliding surface and it is commonly referred as chattering [1].

This is a serious drawback in the sliding mode control utilization as it can degrade the performance of the system, causes stress in the actuators and maximizes control effort [2]. Chattering can be minimized by the use of smooth functions instead of the sign function (like saturation or sigmoidal functions) in first-order sliding modes [3] or by higher-order sliding modes [4].

The use of smooth functions in first order sliding modes has some advantages: reduces chattering and make sliding modes viable in real switches due to their limited switching frequency specially in those systems which employs pulse width modulation with a fixed frequency. The drawback is that it can compromise its robustness and the convergence is made asymptotically to the set point [1][3].

Higher-order sliding mode controllers can reduce and also eliminate the chattering but they may converge asymptotically [1].

In order to satisfy the conditions of convergence to the solution of the system, or the convergence to the sliding regime, it is necessary to define the sliding variable (σ), and a possible arbitrary order sliding variable is [5]:

$$\sigma = \left(\frac{d}{dt} + \lambda\right)^{r-1} \epsilon \tag{1}$$

Where

$\epsilon = x^* - x$;
r: is the degree of sliding surface;
x: vector of state variables;
x^*: references for state variables;
λ: is a constant.

So, the sliding surface is defined as $\sigma = 0$ and the proposed sliding variable differs from (1):

$$\sigma = \int \left(\lambda(\epsilon) + \frac{d}{dt}\right)^{r-1} \epsilon \, dt \tag{2}$$

The difference lies in the integral operator and that λ is a function of $x^* - x$.

In this application, it is considered a sliding surface of order 2 ($r = 2$):

$$\sigma = \int \lambda(\epsilon)\epsilon dt \; + \epsilon = 0 \tag{3}$$

And the function λ is defined as the Gaussian function:

$$\lambda(\epsilon) = k_I \exp(-k_G \, \epsilon^2) \tag{4}$$

II. Brushless DC Motor Electrical Drive

In this paper, the therm brushless DC motor refers to the set composed by an electrical machine, more specifically a surface-mount permanent magnet synchronous machine, with its electric power converter, commonly a three phase machine with a three phase electric converter (a three phase inverter) [6][7]. Ideally, the electrical machine has a trapezoidal back-EMF waveform and with a 120° square wave stator current produces an almost ripple free electromagnetic torque, as in Fig. 1. In this case, the converter operates in six-step mode and with each switch activated by 120° electrical, resulting in 2 inverter legs activated simultaneously.

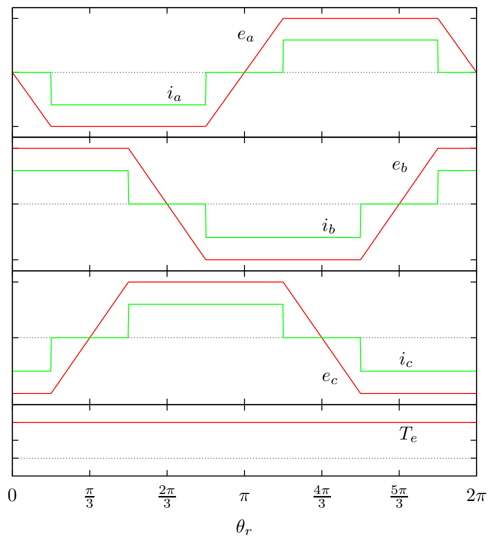

Fig. 1. Brushless DC motor ideal electromagnetic torque generation (θ_r: electrical position of the rotor).

A block diagram of the complete drive system is shown in Fig. 3, where there are two control loops: the stator current control loop, where G_I represents the current loop controller; and the rotor speed control loop, where G_ω represents the speed loop controller. As the time constant of mechanical system is far greater than the time constant of electrical system, those control loops are weakly coupled, so it is possible to make separate analysis for the controllers of speed loop (G_ω) and for current loop (G_I) [8].

The current controller (G_I) is a first order sliding mode controller, as in [9], so its sliding mode variable is:

$$\sigma_I = i^* - i \tag{5}$$

Where

i^*: stator line current reference;
i: measured stator line current:

$$i = \begin{cases} i_a & \text{if } \theta_r \in [30°, 150°[\\ i_b & \text{if } \theta_r \in [150°, 270°[\\ i_c & \text{if } \theta_r \in [0°, 30°[\text{ or } [270°, 360°[\end{cases} \tag{6}$$

And the stator current controller is:

$$G_I: \ \delta = \tanh k_I \cdot \sigma_I \tag{7}$$

Where δ is PWM duty cycle, from -1 (reverse motion) to 1 (direct motion).

The used machine model is as follows:

$$\begin{aligned} \begin{bmatrix} v_a \\ v_b \\ v_c \end{bmatrix} = \begin{bmatrix} L_s & M_s & M_s \\ M_s & L_s & M_s \\ M_s & M_s & L_s \end{bmatrix} \frac{d}{dt} \begin{bmatrix} i_a \\ i_b \\ i_c \end{bmatrix} + \\ R_s \begin{bmatrix} i_a \\ i_b \\ i_c \end{bmatrix} + \begin{bmatrix} e_a \\ e_b \\ e_c \end{bmatrix} + \begin{bmatrix} v_n \\ v_n \\ v_n \end{bmatrix} \end{aligned} \tag{8}$$

Where

e_a, e_b and e_c: induced voltage of stator phases a, b and c, respectively, due to rotor magnets movement, as in (9);
i_a, i_b and i_c: stator phase currents a, b and c, respectively;
L_s: stator phase self-inductance;
M_s: stator phases mutual inductances;
R_s: stator phase resistance;
v_a, v_b and v_c: a, b and c stator phases applied voltages, respectively;
v_n: stator neutral terminal voltage (this terminal is not normally connected).

$$\begin{bmatrix} e_a \\ e_b \\ e_c \end{bmatrix} = \frac{d}{dt} \begin{bmatrix} \Phi_{ra} \\ \Phi_{rb} \\ \Phi_{rc} \end{bmatrix} = \omega_e \begin{bmatrix} \Phi'_{ra} \\ \Phi'_{rb} \\ \Phi'_{rc} \end{bmatrix} \tag{9}$$

Where

Φ_{ra}, Φ_{rb} and Φ_{rc}: linked magnetic fluxes between rotor magnets and stator winding phases a, b and c, respectively;
ω_e: electrical rotor speed.

$$T_e = n_{pp} \left(\Phi'_{ra} i_a + \Phi'_{rb} i_b + \Phi'_{rc} i_c \right) \tag{10}$$

Where

T_e: machine-generated electromagnetic torque;
n_{pp}: number of machine's pole pairs;

The back-EMFs are ideally trapezoidal, therefore Φ'_{ra}, Φ'_{rb} and Φ'_{rc} are also trapezoidal as shown in Fig. 2, considering (9), where Φ_M is their amplitudes and θ_e is the rotor angle in electrical degrees.

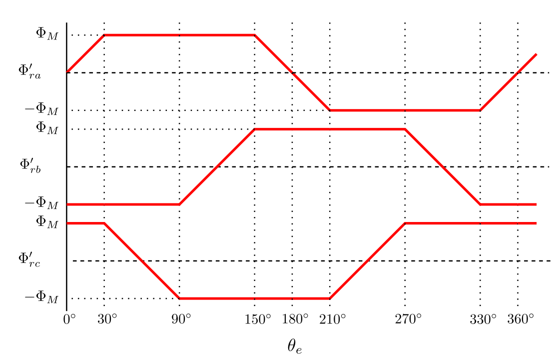

Fig. 2. Waveforms for Φ'_{ra}, Φ'_{rb} and Φ'_{rc}.

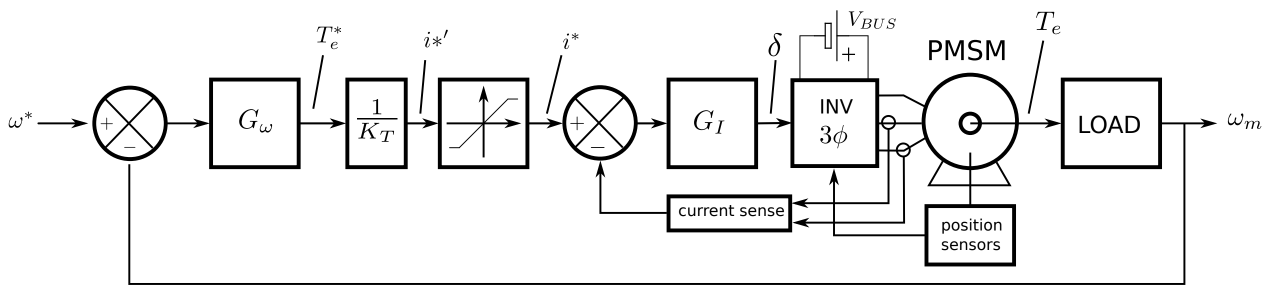

Fig. 3. System complete control block diagram ($K_T = 2n_{pp}\Phi_M$, G_ω: rotor speed controller, G_I: stator current controller).

Considering that only two stator phases are active in each time interval in the six-step 120° power converter mode of operation, the reduced electric equation for machine stator is [9]:

$$v_{12} = 2R_s\,i + 2(L_s - M_s)\frac{di}{dt} + 2\Phi_m\omega_e \qquad (11)$$

Where

v_{12}: voltage between terminals 1 and 2, which can be terminals of a, b or c phases, depending on the rotor position, i. e., as brushless DC motors comprises of a machine and a converter operating in six-step 120° mode, only two phases are feeding the machine each time (neglecting the transient switching between the phases), and a more detailed deduction is shown in[9].

The reachability and the sliding mode conditions of the current controller for the first order sliding mode controller (7) are both shown in [9].

A. Rotor speed loop controller

The speed loop controller is a sliding mode of order 2, as described by the sliding variable (3), so:

$$\sigma_\omega = \int \lambda(\epsilon_\omega)\epsilon_\omega dt + \epsilon_\omega \qquad (12)$$

Where

σ_ω: sliding variable for rotor speed control loop (G_ω);
$\epsilon_\omega = \omega^* - \omega$: shaft speed error;
ω^*: rotor speed reference;
ω: measured rotor speed.

The dynamic mechanical load equation is:

$$\frac{d\omega}{dt} = \dot{\omega} = -\frac{B}{J}\omega - \frac{1}{J}T_L + \frac{1}{J}T_e \qquad (13)$$

Where

B: equivalent frictional coefficient, composed by rotor shaft bearings and load frictional losses;
J: combined inertia momentum of machine rotor and load;
T_L: load torque;

B. System convergence

As a general non-linear system can be written as:

$$\begin{aligned} \dot{x} &= f(x) + g(x)U \\ y &= h(x) \end{aligned} \qquad (14)$$

Where

U: system input;
f, g, h: linear or non-linear functions, characterizing the system;
y: system output.

The system input function can be written as a sum of a continuous function and a switching function:

$$U = U_{eq} + U_c \qquad (15)$$

Where

U_{eq}: is a continuous function and is referred as “equivalent control”, representing the operation point where the sliding regime occurs [10];
U_c: is the switching control, representing the variable structure of the system, responsible to the attractiveness of the system to the sliding regime.

A well accepted method to prove the convergence of that system to the operation point is by the definition of V, a energy Lyapunov function:

$$V = \frac{1}{2}\sigma^2 \qquad (16)$$

For the asymptotic stability of the chosen surface (3) in the equilibrium point ($\sigma = 0$), some conditions must be satisfied:
a) $\dot{V} < 0$ for $\sigma \neq 0$

b) $\lim_{|\sigma|\to\infty} V = \infty$

Condition b is clearly satisfied, but condition a follows:

$$\dot{V} = \sigma\dot{\sigma} \quad \text{and} \quad \dot{\sigma} = \frac{\partial\sigma}{\partial x}\dot{x} \qquad (17)$$

Writing (14) using the defition of the input as in (15):

$$\dot{x} = (f(x) + g(x)U_{eq}) + (g(x)U_c) \qquad (18)$$

Solving U_{eq} to make the first therm of (18) be zero or, in other way, from the definion of equivalent control as the portion of control that is responsible for the set point of the system:

$$U_{eq} = -\left(\frac{\partial \sigma}{\partial x} g(x)\right)^{-1} \left(\frac{\partial \sigma}{\partial x} f(x)\right) \tag{19}$$

Rewritten (17):

$$\dot{V} = \sigma \dot{\sigma} = \sigma \frac{\partial \sigma}{\partial x} g(x) U_c < 0 \tag{20}$$

A simple form of implementing U_c is by signal function (21), however it causes a drawback in system performance due to the so called chattering, which can be considered the main drawback of sliding mode control [11]. But the purpose of the use of signal function here is to show the convergence by proving (20) inequality.

$$U_c = \rho \,\mathrm{sign}(\sigma(x)) \tag{21}$$

Where

ρ: amplitude of switching control input.

Considering the use of function sign in (20):

$$\dot{V} = \frac{\partial S}{\partial x} g(x) \rho \left|\sigma(x)\right| < 0 \tag{22}$$

As the therm $\rho \left|\sigma(x)\right| > 0$, then the reachability condition of the system depends on the internal product of the surface σ partial derivative by x by the function $g(x)$:

$$\frac{\partial \sigma}{\partial x} g(x) < 0 \;\text{ for }\; \sigma \neq 0 \tag{23}$$

The use of a sigmoidal function in (21) does not alter the inequality (23) as well.

In order to prove the sliding mode of the system, one must prove that the equivalent control (19) can be bound to systems limits and in order to prove the reachability condition, (23) must be satisfied. Using (13), the equivalent control of the system input (T_e) is:

$$T_{e_{eq}} = B\omega + T_L \tag{24}$$

Considering the bounding limits of operation, in the maximum desired speed, maximum machine electromagnetic torque must equals the product of maxim speed and shaft friction coefficient plus maximum load torque.

In order to prove the system will stay in the adopted sliding surface (12), (23) leads to:

$$\frac{\lambda(\epsilon_\omega)\epsilon_\omega}{\dot{\omega}} - 1 < 0 \Rightarrow \frac{\lambda(\epsilon_\omega)\epsilon_\omega}{\dot{\omega}} < 1 \Rightarrow \tag{25}$$

$$\lambda(\epsilon_\omega) < \frac{\dot{\omega}}{\epsilon_\omega} \tag{26}$$

So it represents an inequality where the Gaussian function (4) must be inscribed in order to satisfy the reachability condition, where $\dot{\omega}$ can be obtained from (13) for the desired operational situation.

III. Results

The used machine and its load has the parameters shown in Table I. The load torque (T_L) must be kept bellow 2.6Nm for this machine.

TABLE I. BLDC MOTOR AND MECHANICAL LOAD PARAMETERS USED IN SIMULATIONS.

Motor	**Load**
$R_s = 2.3\Omega$	$J = 4.2 \cdot 10^{-3}\mathrm{kg\,m^2}$
$(L_s - M_s) = 12.5\mathrm{mH}$	$B = 3.032 \cdot 10^{-3}\mathrm{kg\,m^2/s}$
$n_{pp} = 3$	
$\Phi_m = 0.12\mathrm{Wb}$	

A. Simulation Results

Some results from simulations are shown in Figs. 4 to 5. In the figures, the load torque is varied abruptly from 0 to its maximum value (2.2Nm) or even to its maximum in the opposite direction (-2.2Nm). Fig. 4 shows the machine accelerating and reaching 1000rpm of operation speed. The details of machine speed is shown in Fig. 5, where its speed decreases when torque load increases and *vice-versa*. Note that the overshot is practically nonexistent and there is no shaft speed steady state error due to the integrative action of the controller, thanks to the selective integral operation given by the introduction of λ as a function of speed error (12). This anti-windup technique is similar to the conditional integration method, where the integrative portion of the controller is activated when the error is bellow of a predefined value [12].

Fig. 6 shows chattering in PWM duty cycle which is applied to the power inverter bridge, which can not be considered as properly a chattering because machine stator current decreases due to inverter bridge phase switching, the controller tries to compensate that by increasing duty cycle.

Fig. 7 shows the machine accelerating from 1000rpm and reaching 2000rpm. During this interval, load torque is applied against machine motion (positive value) and favoring its motion (negative value). Those load torque changes causes some transients in machine speed. After machine achieves its set point speed, it occurs a little overshoot due to load torque favoring its motion (Fig. 8). In $t = 0.35$s, load torque is released, so machine speed falls but integrative action of the controller put it back to its set point. In $t = 0.4$s, a load torque against its motion is applied, so machine speed falls again, but due to integrative action, it reaches its set point after 50ms. When this load is released, machine accelerates but it is back to its set point again in 25ms, in $t = 0.5$s.

B. Implementation Results

The results obtained from the physical implementation are shown in Figs 9 to 11. The former shows the response for a

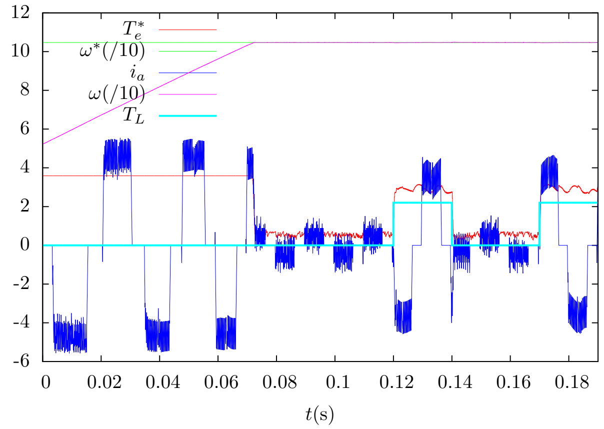

Fig. 4. Machine operation at 1000rpm.

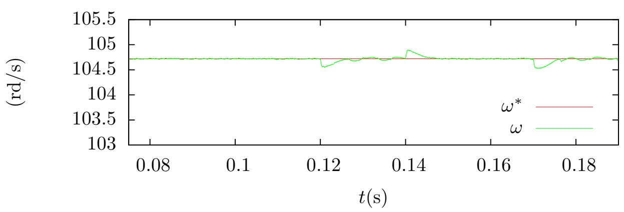

Fig. 5. Machine operation at 1000rpm, detail of speed during load torque transients.

speed step of 60rd/s (573rpm). In that figure, the rotor speed using the proposed second order sliding mode controller, with its integrative action, is shown (ω) together with the results without the integrative action (ω'), i. e., making $k_I = 0$ in (4). The speed without integrative action (ω', $k_I = 0$) presents a steady state error, while the speed with the integrative action (ω, $k_I > 0$) does not present steady state error as expected, but with no overshoot which would be expected for integrative controllers under step responses. The speed error for both situations is shown in Fig. 10, where it is clearly seen that average error using integrative controller is zero. Also, there is no overshoot in rotor speed. In Fig. 9, the electromagnetic

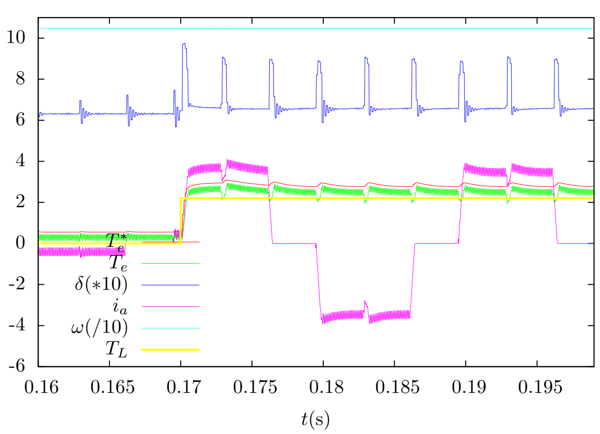

Fig. 6. Machine operation at 1000rpm, detail of PWM duty cycle and reference torque chattering.

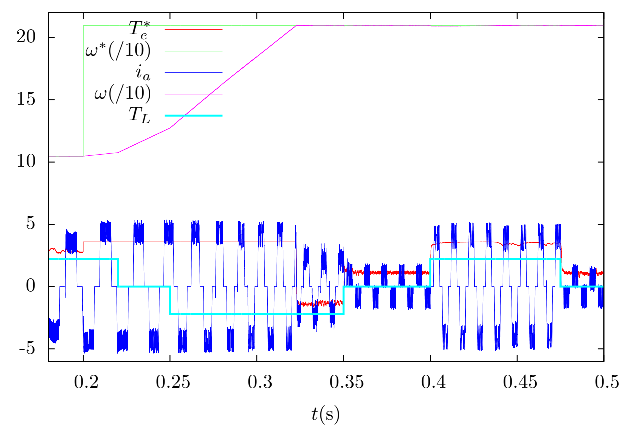

Fig. 7. Machine operation at 2000rpm.

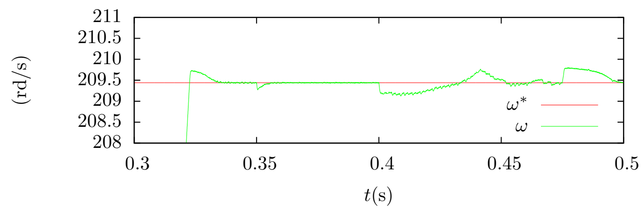

Fig. 8. Machine operation at 2000rpm, detail of speed during load torque transients.

torque reference is also shown.

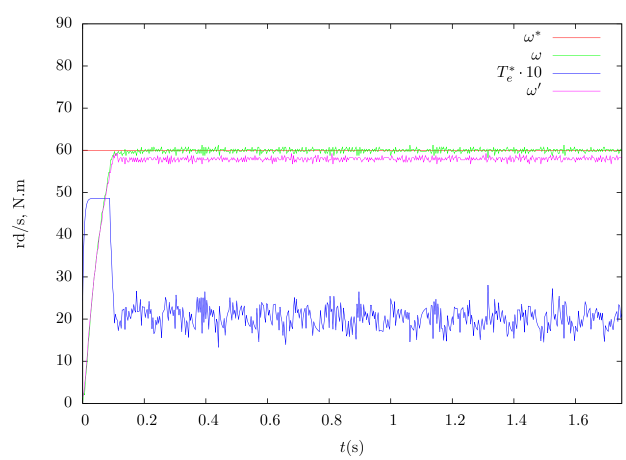

Fig. 9. Machine operation at 60rd/s ($\approx$ 600rpm), show rotor speed with integrative controller action (ω) and without (ω').

Similar results are shown in Fig. 11, where the shaft speed reference is 100rd/s (955rpm). The shaft speed with integrative action (ω) does not present steady state error, while without integrative action (ω') does. The electromagnetic torque reference is also shown (T_e^*).

The implementation setup can be seen in Fig. 12. Basically, the system consists of 2 machines: one is the BLDC motor (4) mechanically coupled to a induction machine (6) used as a generator. Each machines are fed separately by its three-phase inverters (3 and 5). The BLDC motor's inverter is controller

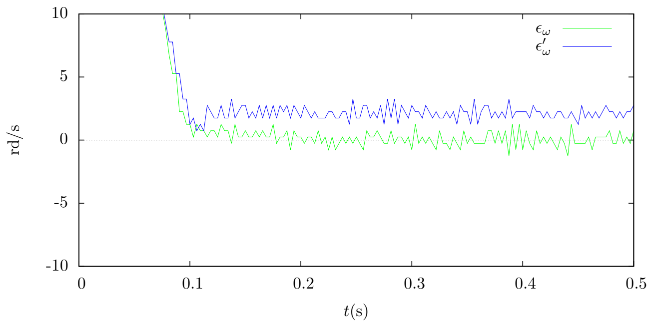

Fig. 10. Error detail of rotor speed with integrative controller action (ϵ_ω) and without (ϵ'_ω).

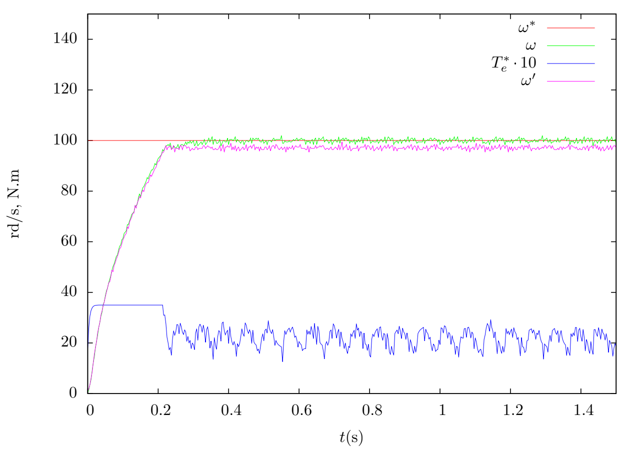

Fig. 11. Machine operation at 100rd/s ($\approx$ 1000rpm), show rotor speed with integrative controller action (ω) and without (ω').

by an ARM Cortex-M4 (2) connected to its PCB while the induction machine's inverter is controlled by an ARM Cortex-M3 which is integrated in its PCB (3).

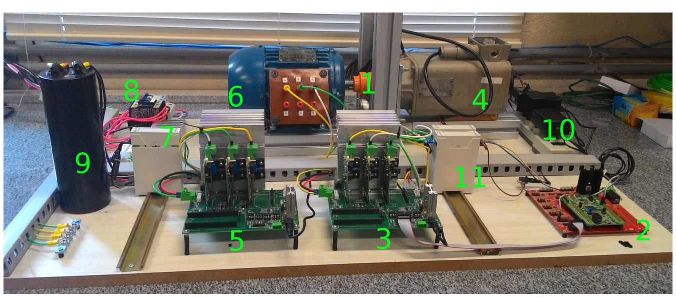

Fig. 12. Implementation setup, where 1: shaft coupling between brushless-DC motor (4) and induction generator (6); 2: ARM Cortex-M4 board; 3: inverter for BLDC motor; 4: BLDC motor; 5: inverter for induction generator; 6: induction generator used as mechanical load; 7: bus rectifier; 8: line input protection; 9: bus capacitor; 10: low voltage circuits power supplies; 11: current sensors.

IV. Conclusions

This work introduces a new sliding mode surface in order to neutralize the steady state error of the system which is introduced by the use of analog functions as switching functions, instead of the signal function. The use of an analog function, as the hyperbolic tangent function, can reduce significantly system chattering, but it is not properly a sliding mode control and causes non-zero steady state error, as pointed out by the literature. The anti-windup effect achieved by the proposed surface is similar to the conventional method called conditional integration, but with the difference that the integrative portion is gradually activated as the error decreases, so the integrator is active even for large error values. This is a good feature once the conventional method can fail if the error does not fall in a limit.

The proposed surface is successfully used in the speed control loop of an electrical machine, a brushless-DC motor, showing a good performance, no steady state error, minimum rotor speed overshoot and reduced chattering. Therefore, the side effects of the use of a sigmoidal function were mitigated.

Acknowledgments

The authors would like to acknowledge the financial support granted by FAPESP (Fundação de Amparo à Pesquisa do Estado de São Paulo) and CAPES.

References

[1] A. J. Fossard and T. Floquet, *Sliding Mode Control in Engineering*, W. Perruquetti and J. P. Bardot, Eds. New York: Maecel Dekker, Inc., 2002, (Chap. 1).

[2] B. Heck, "Sliding mode control for singularly perturbed systems," *International Journal of Control*, vol. 53, no. 4, pp. 985–1001, March 1991.

[3] Y. Shtessel, C. Edwards, L. Fridman, and A. Levant, *Sliding mode control and observation*. New York: Springer, 2014.

[4] I. Fridman and A. Levant, *Sliding Mode Control in Engineering*, W. Perruquetti and J. P. Bardot, Eds. New York: Maecel Dekker, Inc., 2002, (Chap. 3).

[5] J. Slotine and W. Li, *Applied nonlinear control*. Englewood Cliffs: Prentice Hall, 1991.

[6] S. A. Nasar, I. Boldea, and L. E. Unnewehr, *Permanent magnet, relutance, and self synchronous motors*. Boca Raton: CRC Press, 1993.

[7] T. J. E. Miller, *Bushless Permanent-Magnet and Reluctance Motor Drives*. Oxford: Claredon Press, 1993.

[8] B. M. Patre, V. M. Panchade, and R. M. Nagarale, *Sliding Mode Control*. InTech, 2011, ch. Sliding Mode Control of DC Drives, available from: http://www.intechopen.com/books/sliding-mode-control/sliding-mode-control-of-dc-drives.

[9] C. M. R. Oliveira, J. R. B. A. Monteiro, and M. L. Aguiar, "Sliding mode control of brushless dc motor speed with chattering reduction," in *Proceedings of the 2015 IEEE 24th International Symposium on Industrial Electronics (ISIE)*. Búzios, Brazil: IEEE, June 2015, pp. 590–595.

[10] M. Mahmoudi, N. Madani, M. Benkhoris, and F. Boudjema, "Cascade sliding mode control of a field oriented induction machine drive," *The European Physical Journal Applied Physics*, vol. 7, pp. 217–225, 1999.

[11] K. Young, V. Utkin, and U. Ozguner, "A control engineer's guide to sliding mode control," *Control Systems Technology, IEEE Transactions on*, vol. 7, no. 3, pp. 328–342, May 1999.

[12] J. Monteiro2013, W. Pereira, M. Santana, T. Almeida, G. Paula, and I. Santini, "Anti-windup method for fuzzy pd+i, pi and pid controllers applied in brushless dc motor speed control," in *Power Electronics Conference (COBEP), 2013 Brazilian*, Oct 2013, pp. 865–871.